

## STABLE OPERATION OF HHG-SEEDED EUV-FEL AT THE SCSS TEST ACCELERATOR

H. Tomizawa, K. Ogawa, K. Togawa, T. Tanaka, T. Hara, M. Yabashi, H. Tanaka, and T. Ishikawa, RIKEN, SPring-8 Center, Kouto 1-1-1, Sayo, Hyogo 679-5148, Japan  
 T. Togashi, S. Matsubara, Y. Okayasu, and T. Watanabe, Japan Synchrotron Radiation Research Institute, Kouto 1-1-1, Sayo, Hyogo 679-5198, Japan  
 E. J. Takahashi and K. Midorikawa, RIKEN Center for Advanced Photonics, Hirosawa 2-1, Wako, Saitama 351-0198, Japan  
 M. Aoyama and K. Yamakawa, Japan Atomic Energy Agency, Umemidai 8-1-7, Kizugawa, Kyoto 619-0215, Japan  
 T. Sato, S. Owada, A. Iwasaki, and K. Yamanouchi, The University of Tokyo, Hongo 7-3-1, Bunkyo-ku, Tokyo 113-0033, Japan

### Abstract

We completed HHG (Higher-order Harmonic Generation) optical laser-seeded FEL (Free Electron Laser) operation at a 61.2-nm fundamental wavelength with an HHG pulse seeding source from a Ti:sapphire laser at the EUV (Extreme Ultraviolet) -FEL test accelerator. The HHG-seeded FEL scheme must synchronize the seeding laser pulse to the electron bunch. We constructed a relative arrival timing monitor based on EO (Electro-Optic) sampling. Since the EO-probe laser pulse was optically split from the HHG-driving laser pulse, the arrival time difference of the seeding laser pulse, with respect to the electron bunch, was measured in real time. This non-invasive EOS (EO Sampling) monitor made uninterrupted, single shot monitoring possible even during the seeded FEL operation. The EOS system was used for the arrival timing feedback with a hundred-femtosecond adjustability for continual operation of the HHG-seeded FEL. Using the EOS locking system, the HHG-seeded FEL was operated over half a day with a 20 – 30% effective hit rate. The output pulse energy was 20  $\mu$ J at the 61.2-nm wavelength. A user experiment was performed using the seeded EUV-FEL at SCSS, and a clear difference was observed between the SASE FEL and the seeded FEL with a high contrast.

### INTRODUCTION

FEL (Free Electron Laser), which was proposed in the early 1970s, is one of the most promising coherent light sources with arbitrary wavelength [1]. Today, using SASE (Self-Amplified Spontaneous Emission) scheme, FEL is available in wide regions up to hard X-rays [2].

SCSS (SPring-8 Compact SASE Source) [3], which is the prototype FEL machine at SPring-8, was constructed for feasibility tests of new components to realize our FEL machine concept. This SASE FEL generated an EUV (Extreme Ultraviolet) pulse at wavelengths from 50 to 60 nm. This EUV-FEL contributed to a variety of user

experiments, especially research on the resonance absorption of atomic or molecular lines in AMO (Atomic, Molecular, and Optical physics).

SASE starts from shot noise (spontaneous emission) and is amplified through electromagnetic interaction with a high-brightness electron bunch in a single pass (without an optical cavity). Based on this mechanism, the SASE pulse fluctuates in its spectrum due to the temporal multimode. Its spectrum fluctuates shot-to-shot, because of its shot-noise seeding source. The SASE characteristics are not reliable for AMO experiments that aim at a specific wavelength for resonance absorptions. To provide a spectrum with a targeting single peak on the demand of user experiments, a full-coherent seeding source is required instead of shot noise for FEL machines without an optical cavity in shorter wavelengths below the EUV region.

In the methodology, seeding schemes, which have been intensively developed worldwide, are roughly categorized into two kinds of approaches. One is called self-seeding, which utilizes a SASE pulse monochromized just after the first undulator section as the seeding source for the second undulator section by itself [4]. The self-seeding scheme is reliable for seeding in the hard X-ray region.

In the other scheme, an external laser pulse is prepared and directly used as a full-coherent seeding pulse. Up to now, an optical laser can be generated up to the water window region. However, the pulse energy is limited and insufficient for seeding in a shorter wavelength. To extend FEL seeding in a shorter wavelength, this seeding scheme is often combined with HHG (High-Gain Harmonic-Generation) [5]. In the user facility at FERMI (Elettra), the 3rd order harmonic pulse of a Ti:Sapphire laser is used as optical seeding and generates FEL seeded at its 13th harmonics with HHG [6]. For our SCSS, we directly developed external seeding with HHG pulses at the SASE's wavelength. These corresponding HHG's orders of a Ti:Sapphire laser (800 nm) were prepared as follows: 13th (61.7 nm), 15th (53.3 nm), and 17th (47.1 nm).

In 2010, we achieved the first successful seeding at SCSS in the 13th and 15th harmonics [7]. However, the contrast ratio of the pulse energy of the seeded FEL pulses with respect to the SASE background noise was very low (~2). The pulse energy was 1.3  $\mu\text{J}$ , which is not sufficient for resonance experiments in AMO. In addition, the rate of the sufficient seeded FEL pulse was inadequate for user experiments. The seeding conditions varied in a short period. The best seeding conditions did not last more than ten minutes. Accordingly, the quality of our seeding condition was not reliable to be distributed for user experiments.

In this paper, we describe the improvement results of HHG-seeding quality at SCSS EUV-FEL. By applying a relative arrival timing monitor based on EOS (EO Sampling) for timing feedback, sufficient FEL pulses are seeded continuously with narrowband spectra.

### SETUP OF HHG DIRECT SEEDING

In this section, we explain our HHG-seeded FEL setup (Fig. 1), which consists of accelerator that has a variety of beam monitors to check the overlapping conditions and an ultrafast optical laser source, which is the line-locked master trigger of the SCSS test accelerator.

In the direct seeding scheme with an external HHG laser pulse, maximizing the overlap between the seed

laser pulse and the electron bunch is crucial in 6D phase space ( $x, x', y, y', t, E$ ). Here,  $x$  and  $y$  are the horizontal and vertical centroid positions (sizes),  $x'$  and  $y'$  are their momenta (divergences), and  $t$  and  $E$  are the time and the photon energy (central wavelength).

Below, we describe the following technological issue: maintaining the best overlapping conditions between the 50-fs HHG pulse and the 600-fs electron bunch so that they last more than one day.

### SCSS Prototype Accelerator

The SCSS test accelerator consists of a thermionic electron gun, RF bunch compressors (the lowest frequency of RF cavity: 238 MHz), a C-band main Linac, and in-vacuum undulators. The electron is generated at a pulsed thermionic electron gun with a  $\text{CeB}_6$  single crystal cathode. The electron bunches are mainly compressed through a velocity bunching process in the RF bunch compressor cavities and accelerated by a C-band high-gradient Linac up to 250 MeV. At the end, the beam is injected into two in-vacuum undulators with 15-mm period lengths and 300 undulator periods. To suppress the SASE background during the seeding operation by raising the contrast ratio, we used only one undulator. The other important SCSS parameters concerning electron bunch for HHG-seeding operation were a 300-pC bunch charge and a  $\sim 200 \mu\text{m}$  (FWHM) transverse diameter (beam size)

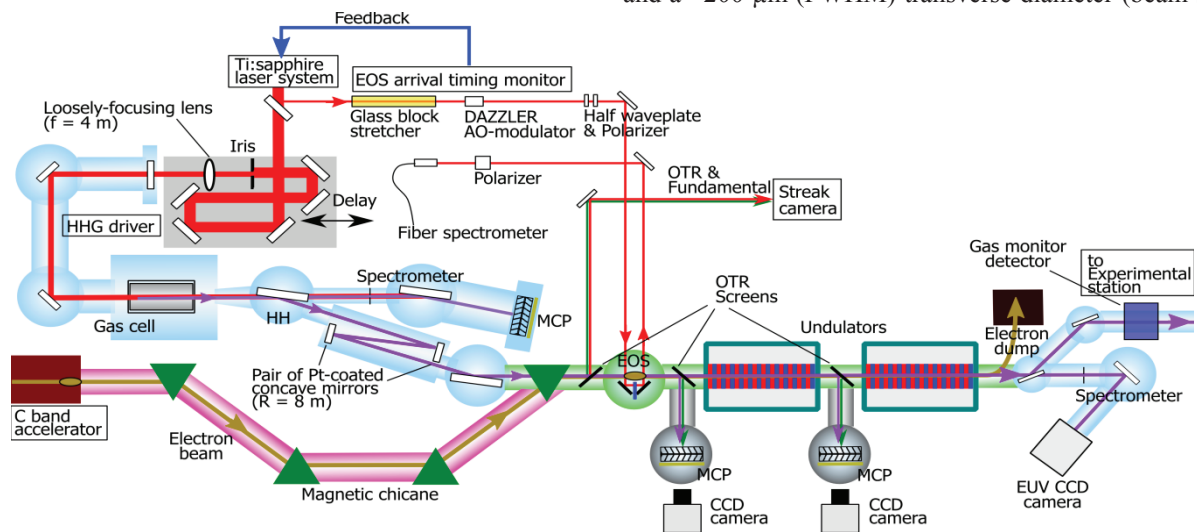


Figure 1: Schematic drawing of HHG-seeding system for EUV-FEL. This seeded FEL system consists of an SCSS FEL machine (accelerator and undulator), a Ti:Sapphire laser system, which is the common laser pulse source for the following HHG-seeding system, and an EOS-based arrival timing monitor. The laser pulse for the HHG-driving and EO-probing was optically split at the accelerator tunnel. HHG pulse was generated in a xenon gas cell with a lens (focal length: 4 m) and separated from the fundamental beam by the first SiC mirror. A pair of Pt-coated concave mirrors with an 8-m curvature radius was used for the loose focusing HHG pulses. Every HHG pulse is selectively reflected by the second SiC mirror, and the seeding pulse should fully overlap the electron bunch at the entrance of the first undulator (undulator 1). The spatial profile of the seeding pulse and the electron bunch on a phosphor screen were measured by MCP at the entrance and end of undulator 1. Temporal overlap was roughly checked by a streak camera. After matching the central wavelength of both SASE and HHG pulses, we utilized the spectrometer at the end of the beamline and installed the arrival timing monitor before undulator 1 by the EOS monitor. Utilizing the EO-probe pulse optically split from the HHG-driving laser pulse, the arrival time difference of the seed laser pulse and the electron bunch was under control and fixed at the optimal seeding condition.

at the entrance of the first undulator. The electron bunch length was stretched to  $\sim 600$  fs (FWHM) to cover the timing jitter between the HHG pulse and the electron bunch. Note that seeding with a longer bunch length also contributes to suppress the level of SASE background.

### Common Laser Source for HHG-driver and EO-probe Pulses

The external optical laser system, which used a driver of the HHG pulse and a probe pulse for the EOS, is based on a chirped pulsed amplification system of a Ti:Sapphire laser (800 nm, 150 fs, 30 Hz). The system consists of a mode-locked oscillator (FEMTOLASERS Produktions GmbH: SYNERGY modified for 238 MHz), which was synchronized to the 238-MHz master clock of the SCSS by feedback locking the cavity length, a regenerative amplifier, and a 4-pass amplifier. The output pulse energy was 100 mJ for the seeding operation. Finally, the pulse was split into HHG-driving laser and EO-probing pulses.

### HHG-seeding Pulse System

The HHG-driving pulse with a pulse energy of 30 mJ was loosely focused by a plano-convex lens (focal length: 4 m) and delivered into the target chamber through a thin window. We set the focus around the entrance pinhole of an interaction cell that was filled with xenon gas. The target gas pressure was adjusted to balance the geometrical phase shift and the harmonic dipole phase. The HHG pulse was selectively reflected with SiC mirrors set at the Brewster angle ( $69^\circ$ ) to allow the fundamental Ti:Sapphire laser through. By introducing a pair of Pt-coated, nearly-normal-incidence mirrors with an 8-m curvature radius, the HHG pulses were loosely focused in the seeding region at the undulator.

After being reflected at the second SiC separator mirror, the HHG pulse was transported by a magnetic chicane into the undulator section. Since the SiC mirrors reflect EUV light above 30 nm, a few orders of HHG including the 13th are selected and sent to the undulator. The HHG-beam diameter at the entrance of the first undulator was  $\sim 500$   $\mu\text{m}$  (FWHM). The pulse energy of the 13th harmonic was estimated to be 2 nJ, which is measured downstream and calibrated by the spectrometer and the gas monitor detector at the end station. The total optical throughput of the HHG transportation was  $\sim 1\%$  (HHG pulse was generated with  $\sim 200$  nJ at the gas cell). The resulting peak power was estimated to be 40 kW in the seeding region, assuming a pulse duration of 50 fs (FWHM).

### Measurement Overlap Between Electron Bunch and HHG Pulse

To optimize the best seeding conditions, the HHG pulses must overlap each other in the 6D phase space. Simultaneously, the HHG wavelength should match that of the SASE radiation. We need a beam diagnostic system to realize maximum 6D overlapping. To obtain higher

FEL gain, both the HHG pulse and the electron bunch are compressed in the 6D volume as much as possible.

The spatial profiles of the seeding pulse and the electron bunch on a phosphor screen were measured by a MCP (multichannel plate) and a CCD camera at the entrance and the end of the first undulator. The system allows simultaneous monitoring of the spatial profiles of the HHG pulse and the optical transition radiation (OTR) from the electron beam to ensure spatial overlap while traveling in the first undulator. The mismatching transverse centroid position and the angle of the direction between the HHG pulses and the electron beams were suppressed into ranges less than 100  $\mu\text{m}$  and 100  $\mu\text{rad}$  by precisely steering the optical path of the HHG pulse independently using the two Pt-coated mirrors.

Temporal overlapping is also crucial for this seeding scheme that requires synchronization of both independent femtosecond-pulsed systems. We chose sequential tuning steps by combining coarse and fine adjustments. At first, the timing difference between the OTR of the electron bunch and the HHG-driving pulse was roughly measured with a streak camera (Hamamatsu Photonics K.K: FESCA-200). Then the timing difference was adjusted with an electrical delay unit of the Ti:Sapphire laser, although it was lowered a certain extent (typically  $<1$  ps). In the second step, the timing was finely adjusted in real time to keep the peak wavelength of the EO signal at the best seeding condition with the feedback program to automatically lock the peak EO signal at the same wavelength.

### Arrival Timing EOS Measurement and Feedback System

We applied the EOS technique as a relative arrival timing measurement in the manner of spectral decoding (Fig. 2). This scheme consists of a probing laser, an EO crystal, a polarizer, and a multi-channel spectrometer for real-time measurements. The EO crystal (ZnTe(110); 3 x 4 x 1 mm thick) was set next to the electron beam, and the EO-probe laser pulse passed through this EO crystal. The probe pulse is linearly chirped and works as a carrier wave. When the electron bunch passes near the EO crystal, the orthogonal polarization components of the

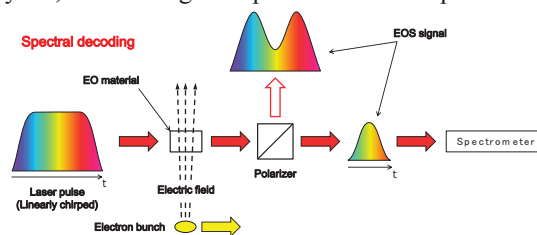


Figure 2: Principal of EO-sampling (EOS) measurement with spectral decoding. This probe pulse is linearly chirped and acts as a carrier wave. The EO crystal is set near the electron beam. The linear polarization of the carrier wave changes into an elliptic polarization in the EO crystal under the electron bunch's electric field. The information of the electron bunches is decoded bunch-by-bunch by spectrometer.

EO-probe pulse are retarded by one against another (birefringence effect) through the crystal under the high electric field of the electron bunch. In this result, the electron bunch timing is encoded as the modulation of the polarization in the spectrum. Then the polarization modulation is converted to intensity modulation in the spectrum by the polarizer. Finally, the carrier wave is decoded by a multi-channel spectrometer in real time. Due to the linear chirp, the profile of the intensity spectrum is equivalent to the temporal laser pulse that corresponds one to one to the electron bunch charge distribution. Our results show that real-time measurement of arrival timing can be realized by monitoring the peak wavelength of the EO-signal's spectrum. The relative timing drift is compensated with a feedback control.

In our EOS system, an EO-probe laser pulse is optically split from the HHG-driving laser at the accelerator tunnel. After splitting, the EO-probe pulse is primarily stretched with a linear chirp to 5 ps through a bulk stretcher made of high-index glass blocks as coarse

tuning. Next, to shape the spectrum flattop and control the higher order of dispersion and the fine stretching factor, we applied an adaptive AO-modulator (FASTLITE: DAZZLER UHR-650-1100) as a fine adjustment tool.

The arrival timing of the electron bunch with respect to the HHG-driver laser pulse is decoded as the spectral peak of the EO signal that corresponds to the electron bunch in the encoding at the EO crystal. The EO signals are decoded by a multi-channel spectrometer (Ocean Optics: QE65000) in an intensity spectrum. The relative timing between the HHG pulse and the electron bunch is fixed at the optimal timing with an automatic feedback system.

Figure 3 shows the spectra of the EO signals. The black line is one of the best seeding conditions as a feedback target. The arrival timing drift appears as the shifting spectral peak position of the EO signals. As shown in Fig. 3, the EO signals in the red and blue lines are 1-ps later and earlier timings to the best timing for the seeding (black line). During seeding, the shift of the peak wavelength is calculated as the drifting time. The amount of timing drift was feedback to the timing delay unit of the Ti:Sapphire laser. Fig. 3-a shows two hours of timing drift. In this case, the total drifting time was about 15 ps. Using our feedback system, the relative arrival timing was kept constant in the timing jitter level of ~200 fs (Fig. 3-b). During user experiments at SCSS, the seeded FEL operated continuously with EOS-feedback over a half day.

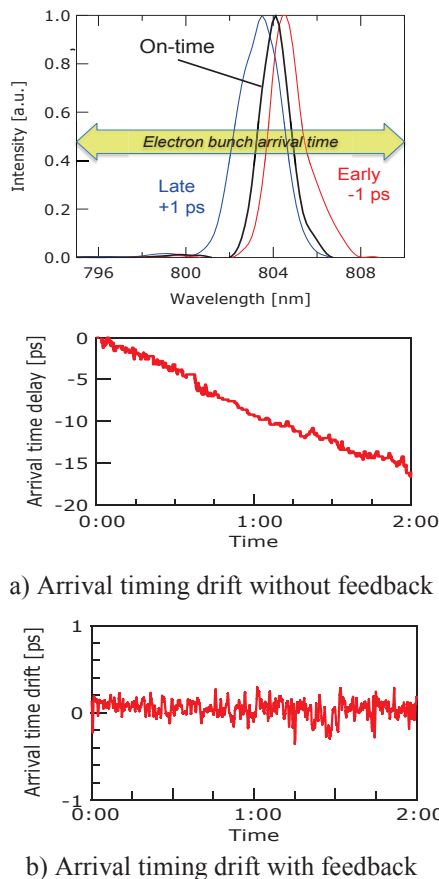


Figure 3: Spectra of EO signals (upper) in different relative timings. Black line is one of the best seeding conditions. Arrival timing drift is calculated automatically by computer program in terms of wavelength position at the peak intensity of the EO signals. Middle figure shows arrival timing drift without feedback. Utilizing our EOS feedback system, arrival timing drift is compensated at a level of timing jitter (lower).

## EXPERIMENTAL RESULTS AND EVALUATION

### Experimental Results of Seeded FEL Spectra

Figure 4 compares the typical spectra of the seeded FEL pulse (red line) and SASE (blue line). The spectral bandwidth of the seeded FEL was 0.06 nm (FWHM). The spectra were single peaks at the peak wavelength with slight fluctuation. We qualitatively evaluated the success rate of the seeding from the fluctuation of the central wavelength and describe it in the following section.

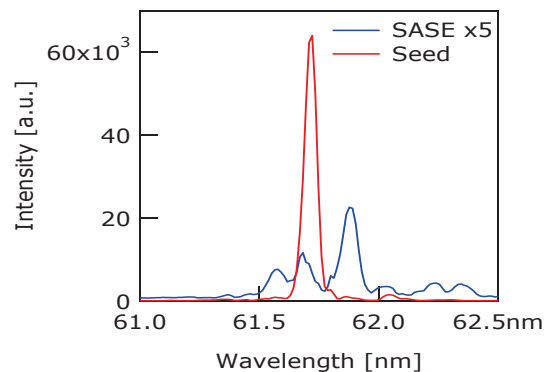


Figure 4: Comparison of the typical spectra of FEL pulses with HHG-seeded operation (red line) and SASE operation (blue line). Spectral bandwidth of seeded pulse was 0.06 nm (FWHM).

*Effective Hit Rate*

For a quantitative evaluation to select a successful seeded FEL pulses, we defined an “effective” hit rate. If the spectral peak intensities of the seeded FEL pulses are larger than four times the standard deviation of the peak SASE intensities, we define the events as an “effective” hit. Successful seeding is characterized with normalization to the standard deviation of the peak SASE intensities in the following formula:

$$\frac{I_{seed} - \overline{I_{SASE}}}{\sigma_{SASE}} > 4$$

where  $I_{seed}$  and  $\overline{I_{SASE}}$  are the peak intensity of the seeded FEL with an effective hit and the averaged peak intensity of SASE, respectively, and  $\sigma_{SASE}$  is the root mean square of the fluctuation. In the case of our former experiment in 2010, according to this definition, the effective hit rate was calculated as 0.3%.

Figure 5 shows the correlation data plot between the normalized intensity and the central wavelength in the data of 10,000 shots with seeded FEL operation in 2012. In Fig. 5, the red points represent the seeded pulses with effective hits, which exceeded  $4\sigma_{SASE}$ . The blue points, which are less than  $4\sigma_{SASE}$ , are defined as the ineffective hits. The central wavelength of the seeded FEL ( $>4\sigma_{SASE}$ ) is distributed from 61.5 to 62.0 nm. On the other hand, the central wavelength in the SASE-like region (blue points) is distributed over 2.5 nm. The standard deviation of the central wavelength is 0.08 nm for the seeded FEL pulse with effective hits ( $>4\sigma_{SASE}$ ). This result resembles the value comparable to the spectral bandwidth of the seeded FEL pulses. Our definition of the effective hit rate is useful to judge the seeding quality in user experiments. For the 10,000 shot data in Fig. 5, the effective hit rate was 24%.

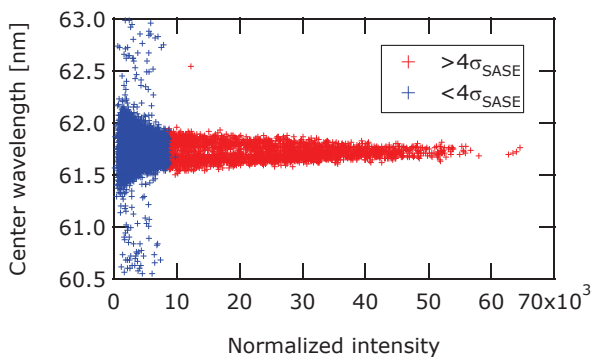


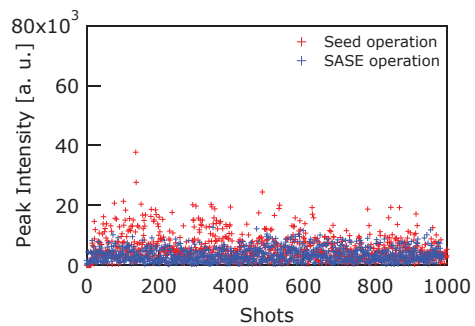
Figure 5: Correlation data plot between normalized intensity and central wavelength with seeded operation. Here,  $\sigma_{SASE}$  is standard deviation of the SASE-FEL intensity fluctuation. Effective seeded FEL pulses are defined as large as  $4\sigma_{SASE}$  (red) for user experiments.

*Improvement results of seeding condition with EOS feedback*

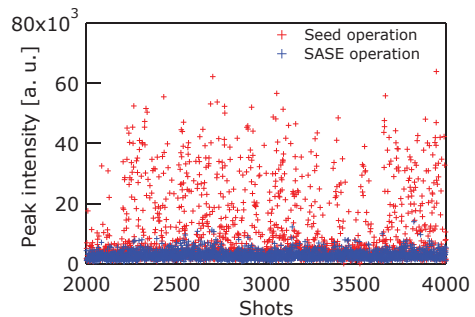
The trend graphs of the peak intensity are shown in Fig. 6. The upper graph (6-a) is our former experimental result from 2010 [7]. In the experimental case, the pulse energy

and the gain of the seeded FEL were limited to 1.3  $\mu$ J and 650, respectively. The lower (6-b) is the result of the seeded FEL operation with feedback based on the EOS measurements. Due to the improvements of the reproducible adjustability and the constant seeding condition maintained with timing feedback, the pulse energy and the gain of the seeded FEL increased significantly to 20  $\mu$ J and  $10^4$ , respectively. In comparison with a) and b), the effective hit rate also increased significantly. In operation with the feedback system, the contrast ratio of the intensity between the seeded FEL and SASE is  $\sim 5$  (peak to peak).

Note that the electron bunch length was increased from 300 to 600 fs from the 2012 seeding experiments to cover the timing jitter between the HHG pulse and the electron bunch. In 2010, we used a 300-fs long electron bunch for seeding. Note the comparison of the results between (a) and (b) in Fig. 6.



a) Peak intensity without EOS-feedback (in 2010: See ref. [7] in detail.)



b) Peak intensity with EOS-feedback (in 2012)

Figure 6: Trend graphs of peak intensities of 10,000 FEL pulses in HHG-seeded operations. Blue and red points are SASE and seeded FEL operations, respectively. Upper graph a) shows experimental results of 2010. Lower b) shows with feedback (2012). Contrast ratio of peak intensity was improved by a factor of  $\sim 3$ . In 2010, seeded FEL pulse energy was 1.3  $\mu$ J. We achieved pulse energy to 20  $\mu$ J.

## SUMMARY AND FUTURE WORK

We demonstrated HHG-seeded FEL with an EOS-based arrival timing monitor. With it, the seeded FEL performance significantly improved for user experiments. Without feedback from the EOS monitor, the continuous operation time of the seeded FEL was limited to less than ten minutes in 2010. Utilizing the feedback system in 2012, the seeded FEL could be operated over half a day. Consequently, operation for user experiments with the seeded FEL was realized at SCSS. Compared to our former seeding condition in 2010, the pulse energy and the FEL gain of the seeded FEL improved from 1.3 to 20  $\mu\text{J}$  to  $10^4$  from 650 (15 times improvement). The effective hit rate was improved from 0.3% to 20-30% (improvements of two orders).

For a higher effective hit rate, we must improve the relative pointing stability in the transverse overlapping. To control the relative pointing, we are planning to install a shingle-shot 3D-BCD (Three-dimensional Bunch Charge Distribution) monitor that was developed at SPring-8 [8]. This monitor, which was developed as an extension of a spectral de-multiplexing EOS monitor, was set to multiple EO crystals around the electron beam axis to measure the higher order of the bunch charge moments as the difference of EO signals from the crystals.

In addition, we are planning to develop a shorter wavelength of the HHG-seeded FEL pulse to the soft X-ray region. To go further in the soft X-ray region, we have to improve the efficiencies of HHG and its transportation by more than ten times. Further compression of both the HHG-pulse and the electron bunch is required for higher FEL gain. With progress for shorter wavelengths, the temporal resolution of EOS and temporal response of EO crystal have to be improved to tens of femtoseconds (FWHM). For this purpose, we are developing a novel EOS system with an organic EO crystal DAST (4-dimethylamino-*N*'-methyl-4'-stilbazolium tosylate) with a temporal response of 30 fs (FWHM) [8].

Our other optional approach is a higher-order harmonic generation in a FEL gain. The higher-order harmonic generation is excited by an increase of bunching factors at higher harmonic frequencies while the fundamental FEL grows [9]. It is known and has been observed that not only odd but also even orders of harmonics are generated off the axis [10]. We demonstrated the 2nd harmonic generation at 30.8 nm in the seeded FEL at 61.5 nm as shown in Fig. 7. At 30.8 nm, the contrast ratio improved to 80. The spectrum has a single peak as a seeded FEL. We believe that it will be a useful light source for user experiments. This scheme is one of the promising approaches as a complementary scheme to provide a high-contrast monochromatic intense FEL pulse even in shorter wavelengths.

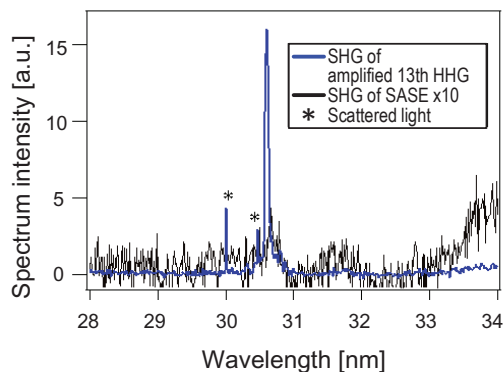


Figure 7: Spectrum of second harmonic seeded FEL lased at 30.8 nm. Contrast ratio is significantly improved to 80 against SASE background.

## REFERENCES

- [1] J. M. J. Madey, "Stimulated Emission of Bremsstrahlung in a Periodic Magnetic Field," *J. Appl. Phys.* **42**, 1906 (1971).
- [2] P. Emma, "First lasing and operation of an ångstrom-wavelength free-electron laser," *Nat. Photonics* **4**, 641 (2010)
- [3] T. Shintake, *et al.*, "A compact free-electron laser for generating coherent radiation in the extreme ultraviolet region," *Nat. Photonics* **2**, 555 (2008).
- [4] J. Feldhaus *et al.*, "Possible application of X-ray optical elements for reducing the spectral bandwidth of an X-ray SASE FEL," *Opt. Comm.* **140**, 341 (1997).
- [5] L.-H. Yu, *et al.*, "High-Gain Harmonic-Generation Free-Electron Laser," *Science* **289**, 932 (2000).
- [6] E. Allaria, *et al.*, "Highly coherent and stable pulses from the FERMI seeded free-electron laser in the extreme ultraviolet," *Nat. Photonics* **6**, 699 (2012).
- [7] T. Togashi, *et al.*, "Extreme ultraviolet free electron laser seeded with high-order harmonic of Ti:sapphire laser," *Opt. Express* **19**, 317 (2011).
- [8] H. Tomizawa, *et al.*, "Non-destructive Real-time Monitor to Measure 3D Bunch Charge Distribution with Arrival Timing to Maximize 3D Overlapping for HHG-Seeded EUV-FEL," *Proceedings of LINAC2012*, 657 (2012).
- [9] Z. Huang *et al.*, *Phys. Rev. E* **62**, 7295 (2000).
- [10] T. Watanabe, *et al.*, "Experimental characterization of seeded FEL amplifier at the NSLS SDL," *Proceedings of FEL2005*, 98 (2005).